Title

Selective trafficking of light chain-conjugated nanoparticles to the kidney and renal cell carcinoma

Authors

Ordikhani, Farideh
Kasinath, Vivek
Uehara, Mayuko
et al.

Publication Date

2020-12-01

DOI

10.1016/j.nantod.2020.100990

Peer reviewed

HHS Public Access

Author manuscript

Nano Today. Author manuscript; available in PMC 2021 December 01.

Published in final edited form as:

Nano Today. 2020 December ; 35: . doi:10.1016/j.nantod.2020.100990.

Selective Trafficking of Light Chain-Conjugated Nanoparticles to the Kidney and Renal Cell Carcinoma

Farideh Ordikhani[1,†], **Vivek Kasinath**[1,†], **Mayuko Uehara**[1], **Aram Akbarzadeh**[1], **Osman A Yilmam**[1], **Li Dai**[1], **Hamza Aksu**[1], **Sungwook Jung**[1], **Liwei Jiang**[1], **Xiaofei Li**[1], **Jing Zhao**[1], **Baharak Bahmani**[1], **Takaharu Ichimura**[1], **Paolo Fiorina**[1,2], **Nasim Annabi**[3], **Reza Abdi**[1,*]

[1]Transplantation Research Center, Division of Renal Medicine, Brigham and Women's Hospital, Harvard Medical School, Boston, MA, USA.

[2]Division of Nephrology, Boston Children's Hospital, Harvard Medical School, Boston, MA, USA.

[3]Chemical and Biomolecular Engineering Department and Center for Minimally Invasive Therapeutics (C-MIT), California NanoSystems Institute (CNSI), University of California - Los Angeles, Los Angeles, CA, USA.

Abstract

Specific delivery platforms for drugs to the kidney and diagnostic agents to renal cell carcinoma (RCC) constitute urgent but unfulfilled clinical needs. To address these challenges, we engineered nanocarriers that interact selectively for the first time with proximal tubule epithelial cells (PTECs) in the kidney and with RCC through the interplay between lambda light chains (LCs) attached to PEGylated polylactic-co-glycolic acid (PLGA) nanoparticles and the membrane protein megalin. Systemic administration of these light chain-conjugated nanoparticles (LC-NPs) to mice resulted in their specific retention by megalin-expressing PTECs for seven days. Repetitive dosing of LC-NPs demonstrated no renal toxicity. LC-NPs also localized selectively to megalin-expressing RCC tumors in mice. Moreover, we confirmed that both the primary tumor and lymph node metastases of human RCC express megalin, reinforcing the potential of LC-NPs for clinical use. Thus, LC-NPs can contribute potentially to improving the management of both non-oncologic and oncologic renal disorders.

[*]Address correspondence to: Reza Abdi, MD, Transplantation Research Center, Brigham and Women's Hospital, 221 Longwood Ave, 3rd Floor, Boston MA 02115, USA. Phone: 617.732.7249; rabdi@rics.bwh.harvard.edu.

[†]These authors contributed equally.

Author Statement

Farideh Ordikhani: Conceptualization, Methodology, Validation, Formal Analysis, Investigation, Data Curation, Writing—Original Draft, Writing—Review & Editing, Visualization. **Vivek Kasinath:** Conceptualization, Methodology, Validation, Formal Analysis, Investigation, Data Curation, Writing—Original Draft, Writing—Review & Editing, Visualization, Funding Acquisition. **Mayuko Uehara:** Investigation. Aram Akbarzadeh: Investigation. **Xiaofei Li:** Investigation. **Osman A. Yilmam:** Investigation. **Li Dai:** Investigation. **Hamza Aksu:** Investigation. **Sungwook Jung:** Investigation. **Liwei Jiang:** Investigation. **Jing Zhao:** Investigation. **Baharak Bahmani:** Investigation. **Takaharu Ichimura:** investigation. **Paolo Fiorina:** Writing—Review & Editing. **Nasim Annabi:** Writing—Review & Editing. **Reza Abdi**—Conceptualization, Methodology, Validation, Resources, Writing—Original Draft, Writing—Review & Editing, Supervision, Project Administration.

Conflict of Interest

All authors declare no conflict of interests.

Graphical Abstract

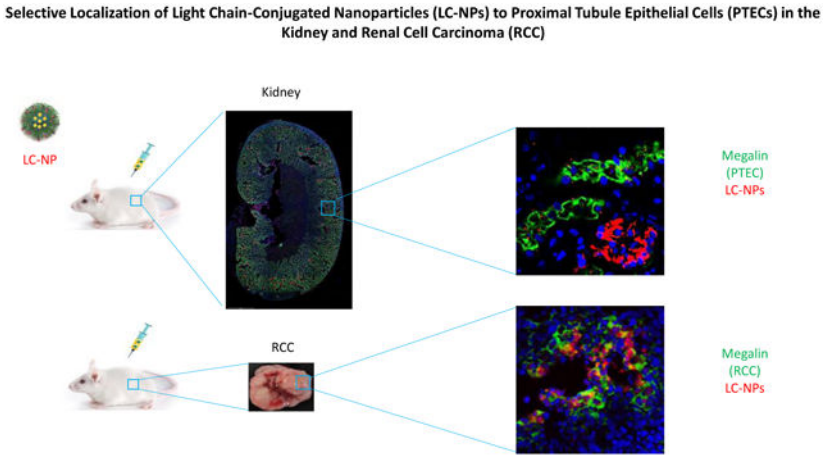

Keywords

Nanoparticles; Light chain proteins; Megalin; Kidney; Renal cell carcinoma

Introduction

Significant anatomical and functional obstacles have hindered the development of selective diagnostic and therapeutic agents that target actively the PTECs of the kidney. Nanomedicine, the delivery of these agents by the use of nanoparticles, offers an enticing solution to this predicament. The potential benefits of nanomedicine include improvement of the pharmacokinetics of a given agent, minimization of systemic toxicity due to its direct delivery to a preferred site, maximization of its dosage at the site of action, and its controlled or triggered release in a spatiotemporal manner [1].

PTECs constitute the lining of the initial urinary space in the kidney, and they are responsible for the majority of re-absorption of ions and small organic molecules from the glomerular filtrate, which clears the urine of almost all proteins [2]. Dysfunction of PTECs contributes to the pathogenesis of several congenital and acquired renal disorders, including polycystic kidney disease (PKD), type II renal tubular acidosis (RTA), and acquired cystic disease of the kidney. In addition, PTECs are the source of the most common clear cell histologic subtype of RCC, which comprises up to 87% of all tumors [3]. Thus, fashioning a method of selective delivery of agents to PTECs may alter the clinical course of these important disorders.

RCC is the sixth most common cause of cancer in men and tenth in women in the United States [4]. A prominent challenge for RCC patients is the high recurrence rate following treatment for localized disease, which ranges between 20–40% [4, 5]. Therefore, the development of a vehicle that can deliver diagnostic agents to RCC would represent a major clinical breakthrough.

Though several previous studies have demonstrated the therapeutic efficacy of drug-loaded nanoparticles to the kidney, very few have featured *in vivo* delivery of nanoparticles conjugated to a molecular recognition entity [6, 7]. One recent publication demonstrated an effective *in vivo* platform of active targeted delivery to the proximal tubule. In this study, Wang *et al.* showed that PEGylated micelles conjugated to the peptide $(KKEEE)_3K$ with an average diameter of 15.0 nm localized specifically to proximal tubules in wild-type mice following intravenous administration [8].

Megalin is a large type 1 transmembrane protein that belongs to the low-density lipoprotein receptor (LDLR) family. It is found on the apical surface of PTECs and is responsible for the reclamation of a variety of filtered proteins from the urine [2]. Along with a central role of megalin in tubular endocytic processes, megalin-deficient mice suffer from tubular resorption deficiency and proteinuria [9]. Besides mere protein clearance from the glomerular filtration, megalin internalizes other molecules, including complexes of vitamins, such as B12, D, and A, their corresponding vitamin-binding proteins, signaling molecules such as angiotensin II and 1–7, albumin, lipoproteins, and thyroid hormones [10–12]. The structure of megalin, as described initially in the rat, is defined by a large luminal portion that contains 36 LDLR ligand-binding complement-type repeat motifs grouped into 4 different domains [2]. Light chains, which are essential components of antibodies, bind to megalin [13].

In this study, we engineered PEGylated PLGA nanoparticles (NPs), to which we attached LCs from human myeloma plasma. The specific binding to megalin expressing cells, abundance and ease of conjugation method make LCs interesting ligands for surface modification of nanoparticles. We hypothesized that these LC-NPs would traffic preferentially to the kidney, where they would undergo internalization by megalin-expressing proximal tubular epithelium. We also predicted that LC-NPs would localize selectively to RCC, a malignancy that arises commonly from PTECs. To our knowledge, no nanocarrier has been synthesized that targets both the kidney and RCC by exploiting the interaction between LCs and megalin. Therefore, LC-NPs would represent an exciting new tool for the delivery of diagnostic agents to the kidney and RCC.

Materials and Methods

Synthesis of nanoparticles

A nanoprecipitation method was used to formulate fluorescent PEGylated-PLGA nanoparticles. Briefly, 5 mg mPEG-PLGA ((Methoxy Poly(ethylene glycol)-b-Poly(D,L-lactide-co-glycolide), Mw: 5,000:30,000 Da, 50:50 LA:GA (w:w)) copolymer (AK102; Polyscitech, USA) and 1 mg PLGA-PEG-Mal ((Poly(lactide-co-glycolide)-b-poly(ethylene glycol)-maleimide, Mw: 30,000–5,000 Da, 50:50 LA:GA (w:w)) copolymer (AI110; Polyscitech) were dissolved in 500 μl acetone (Sigma Aldrich, USA). Then, IRDye 800CW Carboxylate (LI-COR, USA) (IR800) or Alexa Fluor® 488 Dye (Thermo Fisher Scientific) was dissolved in methanol (5 mg/ml). Then we added 50 μl of dye solution to the polymer solution. The resultant solution was added dropwise into 10 ml deionized water containing 1.5 mg polyvinyl alcohol aqueous solution (PVA, Mw ~31,000, Sigma Aldrich) under vigorous stirring. Then, it was stirred for three hours at room temperature in the fume hood

to fully evaporate the organic solvent. Next, the nanoparticles were concentrated and washed by using Vivaspin Centrifugal Ultra Filter tubes (PES Membrane, 10,000 MWCO, Sartorius stedim Lab Ltd., UK). First, we added the nanoparticle suspension to the brims of the Centrifugal Ultra Filter tubes. Following concentration of the nanoparticle suspension to 500 μL in each tube *via* centrifugation at 4°C and 2700 g, we added 500 μL of Dulbecco's Phosphate-Buffered Saline (DPBS; Corning, Manassas, VA) and concentrated the suspension again to 500 μL in each tube. Then, we added another 500 μL of DPBS and concentrated the nanoparticles to 500 μL again. This concentrated suspension represented the nanoparticle suspension (12 mg/mL concentration) used in all the subsequent experiments. All washing steps were performed at 4°C, and the particles were also stored at 4°C.

For microparticle synthesis, the same amounts of polymers (5 mg mPEG-PLGA and 1 mg PLGA-PEG-Mal copolymers) as for the nanoparticle synthesis were dissolved in 500 μl of acetone. Then, 50 μl of IRDye 800CW Carboxylate (5 mg/ml) was dispersed in the polymeric solution. The dispersed phase was emulsified in 10 mL of deionized water containing 50 mg PVA, using a homogenizer for several minutes. Next, the resulting solution was added to 30 mL of 0.15% polyvinyl alcohol aqueous solution (0.15 g PVA in 100 mL deionized water) and stirred for two hours at room temperature in the fume hood. We concentrated and washed the microparticles in Vivaspin Centrifugal Ultra Filter tubes (PES Membrane, 1,000,000 MWCO) in the same fashion as described above for the nanoparticles. The final concentrated suspension represented the microparticle solution used in all the subsequent experiments.

Surface modification of particles was achieved using a covalent linking between maleimide groups on the surface of the particles and sulfhydryl groups on LC proteins (Lambda Light Chains (Free) from human myeloma sera, purified immunoglobulin, ~1.0 mg/mL, ≥99% (electrophoresis), buffered aqueous solution, Sigma-Aldrich). We used Tris(2-carboxyethyl) phosphine hydrochloride solution (TCEP, Sigma-Aldrich, CAS Number 51805-45-9, USA; 0.5 M, pH 7.0 [aqueous solution; pH was adjusted with ammonium hydroxide]) to reduce the LC proteins prior to the conjugation. We added 30 μl of TCEP to 30 μg of LC proteins and incubated them together for 15 min at room temperature. Then, we added the reduced LC proteins to 500 μL of particles (NPs or MPs) and incubated this mixture at 4°C overnight. The ratio of the LC protein to particles is 1:200. Finally, the conjugated particles (LC-NPs or LC-MPs) were washed with 500 μL of DPBS to remove unconjugated LC proteins and concentrated in centrifuge tubes (PES Membrane, 30,000 MWCO, Sartorius stedim Lab Ltd., UK) in the fashion described above. This concentrated suspension represented the LC-NP or LC-MP solution used in all the subsequent experiments.

The size distribution and zeta potential of particles were determined using a Malvern Zetasizer Nano ZS system. The DLS data are reported based on intensity. Measurements were made in triplicates at room temperature, and the nanoparticles were diluted in DPBS prior to measurements. The morphology of the nanoparticles was visualized by transmission electron microscopy (TEM, JEOL 1200EX). Prior to imaging, the freshly prepared nanoparticles were deposited on 200-mesh Formvar/carbon-coated copper grids and

negatively stained with 0.75% uranyl acetate solution for 1 minute and then washed with Milli-Q water.

In vitro biocompatibility evaluation

HK-2 human kidney proximal tubular epithelial cells (PTECs, CRL-2190, adult male donor, American Type Culture Collection) were cultured in RPMI 1640 (GIBCO, USA) supplemented with 10% Fetal Bovine Serum (GIBCO) and 100 μg/mL penicillin-streptomycin. Cells were incubated at 37°C in a humidified atmosphere containing 5% CO_2.

To assess the toxicity of LC-NPs or unconjugated nanoparticles (NPs) on the HK-2 cells by MTT assay, the cells were seeded in each well of a 96-well plate (5×10^3 cells/well). Then, different concentrations of LC-NPs or NPs (6, 30, and 45 μg/ml) were added to each well and incubated for 6, 24, 48, and 72 hours. We did the experiment twice and each time 8 replicates per condition were tested. Cell viability was measured by the Cell Proliferation Kit I (MTT; Millipore Sigma), according to the manufacturer's protocol.

In vitro binding assay

To assess internalization of LC-NPs and NPs, HK-2 cells (3×10^5 cells) were seeded in each well of a 6-well plate and incubated overnight. Then, 100 μl of LC-NPs or NPs loaded with Alexa Fluor® 488 Dye were added to each well (total volume 1 ml) and incubated for one hour at 37°C. After washing with cold DPBS three times, the cells were harvested following digestion by Trypsin-EDTA (0.05%), phenol red (Thermo Fisher Scientific). Then, the cells were incubated with Fixable Viability Dye eFluor® 780 (Thermo Fisher Scientific) diluted 1:1000 in DPBS for 30 minutes at 4°C. The cells were washed with FACS buffer (DPBS + 2% fetal bovine serum +1 mM EDTA + 0.1% sodium azide), prior to performance of flow cytometry using a FACSCanto™ II flow cytometer (BD Biosciences), and the data was analyzed using FlowJo software (FlowJo LLC, Ashland, OR).

To qualitatively measure the cellular uptake of LC-NPs, HK-2 cells were seeded on chamber slides (Thermo Scientific Nunc 154526 Chamber Slide System) at a density of 5,000 cells per well. The cells were incubated with 100 μl of fluorescently labeled LC-NPs, NPs, or DPBS for one hour at 37°C. Then, the cells were washed three times with cold DPBS and fixed in acetone. The cells were stained with primary unlabeled Anti-Lrp2/Megalin antibody (Rabbit polyclonal, Abcam) diluted 1:100 in 3% Bovine serum albumin (BSA, Sigma Aldrich) blocking solution for one hour at room temperature. Then, the cells were incubated with AlexaFluor® 488 goat anti–rabbit IgG secondary antibody (1:400 dilution in DPBS) for 30 minutes at room temperature. Then, slides were washed for five minutes with DPBS and stained with mounting medium with DAPI (VECTASHIELD, Vector Laboratories Burlingame). Samples were subsequently visualized using an Evos™ FL Auto 2 by Invitrogen (ThermoFisher Scientific) fluorescence microscope.

In vivo biodistribution studies

Animal studies were approved and conducted, according to the Institutional Animal Care and Use Committee of Brigham and Women's Hospital, Boston, MA. For tissue biodistribution studies, C57BL/6 (JAX#000664, male and female, 7–8 weeks) or BALB/c

(JAX# 000651, male, 7–8 weeks) mice received a single intravenous injection of 100 μl of either LC-NPs or NPs loaded with IRDye 800CW Carboxylate at the same particle concentration (n=3–4 mice per group). Of note, for all the biodistribution studies, we divided the NP suspension in half. Half of the NPs were conjugated with LC proteins (LC-NPs), and the other half was kept as non-conjugated NPs. Immediately, and 1, 2, 7, and 28 days following injection, the mice were euthanized and perfused with DPBS, and their major organs were harvested and imaged by using a UVP iBOX Explorer Imaging Microscope (UVP) equipped with a 750–780 nm excitation filter and an 800 nm long-pass emission filter. MFI for each organ was calculated by ImageJ (National Institutes of Health; Bethesda, MD) with constant brightness values for each. Three mice were also injected with free IRDye 800CW Carboxylate dissolved in PBS at the same concentration as the amount encapsulated by the LC-NPs and NPs, and the dye distribution was assessed one day post-injection.

Biodistribution studies in tumor-bearing mice

A suspension of 100,000 Renca (ATCC® CRL-2947™) cells in 50 μL of DPBS was implanted inside the capsule of the right kidney of BALB/c mice, using a technique described previously [14]. Briefly, mice were anesthetized with Isoflurane, and an incision was made below the ribs and parallel to the spine. The kidney was extracted and immobilized with a cotton tip, and kept moisturized with sterile DPBS. The single-cell suspension was gently implanted into the kidney capsule by a syringe with a 30-gauge needle. The injection site was located at the upper and/or lateral side of the kidney to avoid damage to the major blood vessels. The glass tip was slowly pushed into the capsule toward the inferior pole of the kidney, as far as possible to avoid perforating the kidney capsule in other areas. The cell suspension in 50 μL of PBS was inserted under the kidney capsule, and the fine tip was pulled out of the kidney capsule slowly to avoid cell leakage. The kidney was returned into the body cavity. Finally, the abdominal wall was closed with a two-layer suture. Three weeks post-implantation, the mice received a single intravenous injection of either LC-NPs or NPs loaded with IRDye 800CW Carboxylate at the same particle concentration (n=3–4 mice per group). 1, 2, and 3 days post-injection, the mice were euthanized and perfused with DPBS, and their major organs and lymph nodes were harvested for imaging, as previously described. The right kidney lymph node, identified as we have previously described [15], was designated as the draining lymph node (DLN). The kidney lymph node is a single lymph node that drains each kidney, and it is located medial to the kidney. The left kidney lymph node was considered as the non-draining lymph node (NDLN).

Cilastatin treatment

For the *in vivo* experiment, female C57BL/6 mice were divided into two groups. The first group (n=3–6) was treated subcutaneously with 100 mg/kg cilastatin sodium salt (≥98%, Sigma Aldrich, USA) once daily for 4 days, and the second group (n=3–6) was treated subcutaneously with vehicle (DPBS) for 4 days. On the day of the last treatment, either unconjugated NPs or LC-NPs were injected to the mice. One day post injection, the mice were euthanized and perfused with DPBS, and the kidneys were harvested and imaged.

For the *in vitro* experiment, 10,000 HK-2 cells were cultured in chamber slides (Thermo Scientific Nunc 154526 Chamber Slide System) and treated with cilastatin (10 mg/ml) or an equivalent volume of DPBS for one hour. Then, the cells were washed with DPBS twice, and both groups of cells were incubated with the same amount of LC-NPs (100 μl) for another one hour at 37°C. Next, the cells were washed twice with cold DPBS and stained with ReadyProbes™ Cell Viability Imaging Kit-Blue/Green (#R37609, Invitrogen). Images were captured by Evos™ FL Auto 2 by Invitrogen. Several random fields were used for quantification of LC-NPs in each sample.

Megalin knockdown using siRNA

Megalin siRNA (sc-40103, SCBT) and control siRNA (sc-73007, SCBT) (100 nM) were mixed with transfection reagent Lipofectamine 2000 (11668019, Invitrogen) at room temperature for 10 min and then added to HK-2 cells. After 48 hours, megalin knockdown efficiency was confirmed by Western blot. The primary antibody anti-megalin (ab76969, abcam) was used at 1:1000 dilution, and the secondary antibody anti-rabbit HRP (ab6721, abcam) was used at 1:2000 dilution. 48 hours following transfection, 10,000 HK-2 cells were cultured in chamber slides and incubated with 100 μL of LC-NPs (12 mg/ml) containing IR800 for one hour at 37°C. Then, the cells were washed with cold DPBS twice and fixed with 1% paraformaldehyde. DAPI was used to counterstain the cell nuclei. The stained cells were visualized using an Evos™ FL Auto 2 by Invitrogen.

Histology and immunofluorescence imaging

Following UVP iBOX Explorer Imaging, the kidneys and tumors were immediately frozen and embedded in optimum cutting temperature (OCT) compound (Tissue Tek, Sakura Finetek, Torrance, CA, USA). The frozen kidneys were cut into 8-μm sections with a cryomicrotome. Then, the sections were fixed in cold acetone for 10 minutes at room temperature, followed by immersion in 3% Bovine serum albumin (BSA, Sigma Aldrich) blocking solution. The sections were incubated overnight at 4°C with primary antibodies, including anti-CD31 Antibody (colon MEC13.3, Biolegend), anti-Lrp2/megalin antibody (Rabbit polyclonal, abcam), anti-podoplanin antibody (Polyclonal Goat IgG, R&D Systems), fluorescein-labeled Lotus tetragonolobus lectin (LTL, Vector Laboratories), and Mouse TIM-1/KIM-1/HAVCR Antibody (Polyclonal Goat IgG, R&D Systems) followed by incubation with secondary antibodies (AlexaFluor® 488 goat anti–rabbit IgG, AlexaFluor® 488 goat anti–rat IgG, and AlexaFluor® 594 Rabbit anti-Goat IgG, all from ThermoFisher Scientific) for 30 minutes at room temperature. The primary antibodies were diluted 1:100 in 3% BSA-DPBS, while the secondary antibodies were diluted 1:400 in DPBS solution. Slides were washed with cold DPBS for several minutes, stained with DAPI, and coverslipped for fluorescence microscopy imaging.

For hematoxylin and eosin (H&E) staining, tissues were fixed in 10% formalin solution and embedded in paraffin blocks. Sections were cut and stained with H&E by conventional techniques.

Slides containing paraffin-embedded sections of RCC primary tumor and lymph nodes with metastatic RCC (clear cell type) from human patients (n=5 patients) were obtained from

Dana-Farber/Harvard Cancer Center Pathology Core with IRB approval (#2018P000905/PHS). Tumor paraffin sections were deparaffinized and antigen retrieved by treatment with 0.1 M Citrate buffer pH 6.0 in a pressure cooker, then washed in DPBS. After blocking with 3% BSA-DPBS, sections were incubated with rabbit anti-human megalin antibody (ab236244; Abcam, Cambridge, MA) at 1:200 dilution in 3% BSA-DPBS. The sections were incubated with anti-rabbit Alexa 488 antibody (1:400 dilution) or anti-goat Cy3 antibody (Jackson immunochemicals) for 30 minutes and washed. Vectashield (Vector Laboratories, Burlingame, CA) containing DAPI was applied and the slides were cover-slipped. Fluorescent images were obtained with a Nikon EZ-C1 confocal microscope.

Long- and short-term safety of LC-NPs

To study renal toxicity, C57BL/6 mice of 7–8 weeks of age received a single intravenous injection of 100 μl of either LC-NPs or NPs at the same particle concentration (12 mg/ml) (n=4 mice per group). Separately, 4 mice were injected with an equal volume (100 μl) of vehicle (DPBS). 1, 7, and 28 days following injection, the blood was collected, and the blood urea nitrogen (BUN) was measured by the Infinity Urea kit (Thermo Fisher Scientific) and compared against a standard BUN solution of 100 mg/dL (Sigma-Aldrich) using a VersaMax microplate reader (Molecular Devices Corp., Sunnyvale, CA), as per the protocol provided by Thermo Fisher Scientific. This experiment was repeated in another set of 7–8 week-old C57BL/6 mice (4 mice/group). Blood was collected 1, 7, and 28 days following injection, and the serum was separated by centrifugation. The creatinine (Cr) of the serum was measured, according to the instructions provided in the Mouse Creatinine Assay Kit (Crystal Chem, USA).

To study the long-term renal safety of LC-NPs, 5 mice underwent intravenous administration of 100 μl of LC-NPs (12 mg/ml) weekly for one month. Their serum was collected at the end of the month, and their BUNs were measured by the method mentioned above.

Statistical Analysis

A two-tailed Student’s t-test or one-way ANOVA was used to determine statistical significance between two groups and several groups, respectively, by using GraphPad Prism 5.0. Data represent means ± SD. *$P<0.05$*; **$P<0.01$*; ***$P<0.001$*; NS: not significant.

Results

Characterization of LC-NPs

We used a nanoprecipitation method to assemble NPs from mPEG-PLGA (Methoxy Poly(ethylene glycol)-b-Poly(D,L-lactide-co-glycolide)) and mPEG-PLGA-Mal (Poly(lactide-co-glycolide)-b-poly(ethylene glycol)-maleimide) copolymers (Fig. 1A). This method resulted in the synthesis of monodispersed spherical PEGylated NPs (as seen in Fig. 1B) with hydrophilic surface coating. The maleimide functional groups on the surface of PEGylated PLGA NPs allow LCs to be conjugated through thiol–maleimide reactions. Prior to conjugation, the disulfide bonds in the LCs were reduced with TCEP, an efficient, thiol-free, odorless reducing agent that displays high stability within a wide range of pH [16]. Reduction of the cysteine residues in the LCs yields free thiol groups, which can bind to

maleimide on the surface of the NPs. The toxicity of LC-NPs to HK-2 PTECs was evaluated by MTT assay over time. As shown in Fig. 1C, the viability of LC-NP-treated cells at each time point was higher than 95%, demonstrating that LC-NP is biocompatible and exerts low cellular toxicity. Moreover, incubation of HK-2 cells for 24 hours with a gradient of concentrations of either NPs or LC-NPs demonstrated no significant difference in viability, as assessed by MTT assay (Fig. 1D). Similarly, no significant difference in viability was observed after 6, 48, or 72 hours of incubation with a gradient of concentrations of either NPs or LC-NPs (Fig. S1).

Next, LC-NPs were loaded with a fluorescent dye to assess their trafficking and retention. IR800 dye was chosen as the fluorophore, as its emission wavelength minimizes autofluorescence with enhanced signal recovery and a high target-to-background contrast [17, 18]. PEG-PLGA NPs containing IR800 with an average hydrodynamic diameter of 77.8 ± 0.5 nm and polydispersity index (PDI) of <0.2 by dynamic light scattering (DLS) were synthesized. IR800-NPs were conjugated with LCs (LC-NPs). DLS measurements following LC conjugation displayed a slight increase in the size of LC-NPs to 79.7 ± 0.1 nm. The hydrodynamic diameter of a nanoparticle is often larger than the core diameter, due to the addition of a hydrodynamic layer through surface modification and the formation of a hydration layer in aqueous solution. The measured core diameter of unconjugated NPs and LC-NPs were 27.9 ± 6.8 nm and 28.3 ± 7.8 nm, respectively. The zeta potentials of the unconjugated NPs and LC-NPs were −4.85 ± 0.4 and −3.19 ± 0.5 mV, respectively. The relatively neutral (± 10 mV) zeta potential of both LC-NPs and NPs can reduce interactions with the mononuclear phagocytic system, prolong circulation time in the systemic vasculature [19], and confer likely low repulsion by the charge-selective, negatively charged slit diaphragm between podocytes in the glomeruli of the kidney.

To evaluate the applicability of LC-NPs as a targeting vehicle for the kidney, we characterized the expression of the transmembrane protein megalin microanatomically through immunofluorescence staining, which confirmed its restriction to the proximal tubule (Fig. 1E). Megalin was expressed highly and situated at the apical surface of PTECs in the kidney as expected [2], indicating its remarkable potential as a target for the trafficking and accumulation of LC-NPs.

Internalization of LC-NPs by PTECs was then confirmed by both qualitative and quantitative measures *in vitro*. Incubation of HK-2 PTECs with either LC-NPs or unconjugated NPs for one hour resulted in higher uptake of LC-NPs by PTECs in comparison to control NPs (Fig. 1F–G). Moreover, flow cytometric analysis confirmed a significantly higher presence of LC-NPs in PTECs, as compared with NPs (Fig. 1H).

In vivo targeting and biodistribution of LC-NPs

The efficacy of LC-NPs to target the kidney was studied in healthy C57BL/6 mice. *Ex vivo* optical imaging of murine kidneys demonstrated higher accumulation in the kidneys of LC-NP-treated mice compared to the mice that received a single intravenous injection of NPs or PBS (Fig. 2A). Higher mean fluorescence intensity (MFI) signal in the kidneys was observed up to 7 days following a single intravenous injection of LC-NPs, as compared to the mice that received NPs (2.7-fold higher at 1 day, 3.4-fold higher at 2 days, and 2.2-fold

higher at 7 days post-injection) (Fig. 2B). *Ex vivo* organ imaging revealed that the kidneys were cleared of both LC-NPs and NPs at 28 days post-injection (Fig. 2A–B). We also studied the clearance of free IR800 dye *in vivo*, which underwent full renal clearance in 24 hours, demonstrating that the fluorescent signal detected in the kidneys during the first seven days represented primarily the retention of LC-NPs.

The distribution of LC-NPs to major organs was determined by fluorescence imaging. *Ex vivo* imaging 24 hours following intravenous injection of fluorescently labeled LC-NPs revealed that most LC-NPs accumulated in the kidney, the lung and liver had the second highest signal level, and the signal was negligible in all other major organs (Fig. S2A).

The distribution of LC-NPs inside the kidney was determined by immunofluorescence staining. Localization of LC-NPs was negligible in the glomeruli 24 hours following intravenous injection in C57BL/6 mice (Fig. 2C–D). In contrast, a large number of LC-NPs localized predominantly to the apical surface of the PTECs in the kidney, as determined by their position between the LTL^+ or $megalin^+$ apical membrane and the nuclei of the cells (Fig. 2E–F).

Moreover, LC-NPs localized selectively to the proximal tubules of the kidney and were stable for up to 7 days post-injection, as demonstrated by *ex vivo* imaging and immunofluorescence staining. Representative fluorescence micrographs of the kidneys at 1, 2, and 7 days following a single intravenous injection of LC-NPs are shown in Fig. S2B–D.

Next, we sought to interrogate the mechanism by which LC-NPs traffic to the PTECs in the kidney by testing our hypothesis that it is filtered by the glomerulus into the urinary space and tubular lumen. Therefore, we studied the trafficking of IR800-loaded microparticles (MPs) with spherical morphology and an average size of 6.12 ± 1.4 μm (Fig. S2E) to the kidney *in vivo*, in order to confirm the size restriction imparted by the fenestrated endothelium and slit diaphragm in the glomerulus to accumulation of LC-NPs in the proximal tubule as well as to monitor for any nonspecific uptake of light chain-conjugated particles by peritubular capillary endothelial cells in the kidney. As shown in Fig. S2F, MPs and LC-MPs accumulated in the lung, and no trafficking was observed to the kidney, a finding that supported our hypothesis regarding the size-selective property of localization by NPs to the proximal tubule, conferred by their requirement for glomerular filtration.

Long- and short-term safety of LC-NPs

Next, we evaluated if the administration of LC-NPs would cause damage to the kidney, as LCs can be toxic to the tubular epithelium [20–22]. As shown in Tables 1 and 2, the renal function of C57BL/6 mice injected with either LC-NPs or NPs, as assessed by BUN and serum Cr, respectively, resembled the levels of normal female C57BL/6 mice tested in our laboratory (BUN of 12–18 mg/dL and serum Cr of 0.13–0.15 mg/dL) through 28 days following injection, confirming the safety of LC-NPs. Furthermore, histopathological evaluation of the kidney demonstrated negligible long-term changes in glomerular and proximal tubular architecture for up to 28 days post-injection (Fig. 3A). Moreover, the absence of kidney injury molecule-1 (KIM-1), an established marker of proximal tubular

damage, at 7 days following injection (Fig. 3B) and the other time points (data not shown) confirmed the lack of significant toxicity.

To study the safety of repetitive treatment with LC-NPs, C57BL/6 mice received intravenous injections of LC-NPs weekly for up to one month. The measured BUN was comparable with the normal BUN range for C57BL/6 mice. The H&E staining of the kidney tissue revealed no change in morphology, as shown by the representative light micrographs in Fig. 3C. Furthermore, KIM-1 staining showed no sign of damage to the proximal tubules of the kidney (Fig. 3D).

Megalin-mediated uptake of LC-NPs in PTECs

Notably, observation of LC-NPs in the urine immediately after injection by TEM (Fig. 4A), seen clearly in comparison to the urine of a naïve mouse (Fig. S3A), provided further evidence that LC-NPs undergo swift filtration by the glomerulus. Immunofluorescence staining of the kidney tissue immediately post-injection confirmed the presence of LC-NPs along the apical surface of the megalin-expressing PTECs (Fig. 4B).

We hypothesized that the accumulation of LC-NPs in the PTECs of the kidney is dependent on its binding to megalin. To test this hypothesis, we treated the mice subcutaneously with cilastatin or vehicle (DPBS) once daily for 4 days, prior to injection of either NPs or LC-NPs. Cilastatin, an inhibitor of renal dehydropeptidase-I (DHP-I), blocks megalin-mediated uptake in the kidney through competitive inhibition [23]. The mice were euthanized 24 hours after intravenous injection of either NPs or LC-NPs, and the kidneys were harvested for imaging.

Representative *ex vivo* images of the kidneys are shown in Fig. 4C–D. The MFI signals from the kidneys of the mice treated with cilastatin were significantly lower than the MFI signals of the kidneys from mice treated with vehicle (Fig. 4E), indicating lower retention of LC-NPs in cilastatin-treated mice in comparison to the vehicle-treated mice. Moreover, no statistical difference was observed between vehicle- and cilastatin-treated mice when the mice were injected with NPs (Fig. 4E). This supported our hypothesis that the accumulation of LC-NPs in the kidney was dependent on their binding to megalin. Next, we examined the specific effect of cilastatin on the binding of LC-NPs to PTECs by treating HK-2 human PTECs *in vitro* directly with LC-NPs and cilastatin. As shown in Fig. 4F, the number of LC-NPs that underwent uptake by HK-2 cells following treatment with cilastatin was significantly lower in comparison to HK-2 cells that did not receive cilastatin. Next, we performed effective knockdown of megalin expression in HK-2 cells, using siRNA directed against the megalin gene. HK-2 cells treated with megalin siRNA exhibited significantly lower internalization of LC-NPs than the cells treated with the control siRNA (Fig. 4G).

In vivo biodistribution of LC-NPs in renal cell carcinoma-bearing mice

In consideration of the selective trafficking of LC-NPs to megalin-expressing PTECs, we next evaluated the efficacy of LC-NPs to target renal cell carcinoma in murine RCC (Renca) tumor-bearing mice. The Renca cell line is derived from renal cortical carcinoma in mice of Balb/C background, and we injected these cells inside the right kidneys of these mice. NPs or LC-NPs were administered intravenously to RCC tumor-bearing mice, which were then

euthanized 1, 2, or 3 days following injection. Remarkably, the LC-NP-treated mice exhibited higher tumor accumulation compared to NP-treated mice at each time point (Fig. 5A). Representative images of kidneys with the RCC tumor from sacrificed mice at each time point are shown in Fig. 5B. Injection of LC-NPs resulted in identification of the exophytic masses in the kidneys infiltrated by RCC, which contained a higher signal in comparison to the contralateral kidneys that were not injected with RCC, as seen in the representative photograph and *ex vivo* image (Fig. 5C).

Then, we studied the targeting efficacy and retention of LC-NPs in draining kidney lymph nodes (DLNs) and non-draining kidney lymph nodes (NDLNs) of RCC tumor-bearing mice up to three days post-injection of a single dose of either LC-NPs or NPs. As expected, the DLNs of the mice injected with LC-NPs contained a higher signal compared to the DLNs from mice that received NPs (Fig. 5D). Moreover, the DLNs contained a higher signal compared to NDLNs, 3 days following injection of RCC tumor-bearing mice with LC-NPs (Fig. 5E). Renca tumor cells express high level of megalin as shown in Fig. S3B. Immunofluorescence staining of tumor tissue demonstrated co-localization of LC-NPs with megalin-expressing cells in murine tumor tissue (Fig. 5F).

Finally, we assessed if human RCC also expresses a high degree of megalin to confirm the translatability of LC-NPs. Indeed, we found that human RCC tumors (clear cell type) from 5 different patients expressed a high level of megalin (Fig. 5G and Fig. S3C). Furthermore, we found that metastatic lesions of RCC in DLN biopsies of 5 affected human patients also exhibited robust expression of megalin (Fig. 5H and Fig. S3D), demarcating these lesions clearly from the surrounding lymph node stroma.

Discussion

The field of nanomedicine constitutes a promising new frontier in nephrology research. The development of targeted drug carriers to PTECs can alter fundamentally the management of patients with oncologic, congenital, and acquired diseases of the kidney that arise from these cells. Nanomedicine can make a particularly prodigious impact in the management of RCC, as NPs loaded with contrast agents or dyes can be used as a means for increasing the sensitivity for detection of subclinical malignancies and metastatic lesions. Hence, nanocarriers can be harnessed to solve the current, exigent, and unmet clinical needs for precision medicine and sensitive diagnostic agents in the practice of nephrology.

The size, shape, and charge of NPs together affect their ability to localize to various compartments within the kidney [6, 7], representing significant obstacles in their delivery. The distance between the cell membranes of adjacent podocytes is estimated to be 39 nm [24], and interdigitating molecules of nephrin and nephrin-like protein 1 project into the space between these podocytes, forming heterogenous pores of varying sizes and shapes that together comprise the negatively-charged slit diaphragm [24, 25]. The slit diaphragm and the intricate meshwork that covers the fenestrations in renal peritubular capillaries can prevent the access of NPs to the tubules in the kidney. Though the most recent study measures the pore size between the protein strands comprising the slit diaphragm as no larger than 15 nm in any dimension [26], nephrin and nephrin-like protein 1 fibers are thought to function like

"molecular springs" that are distensible [24, 27]. In addition, classic experiments by Barry Brenner's group also demonstrated the importance of glomerular transcapillary flow and pressures in the determination of solute clearance from the blood [28]. Therefore, filtration of particles with radii greater than 15 nm could be possible through the flexible fibers that constitute the slit diaphragm through the force of convection provided by the blood flow in the glomerular capillaries.

In this study, we synthesized for the light-chain conjugated PLGA NPs (LC-NPs) specifically designed to target the membrane protein megalin, which is expressed both by the proximal tubular epithelium in the kidney as well as RCC cells. We demonstrated that LC-NPs localized selectively to both of these cell types *in vitro* and *in vivo*. PLGA is a biodegradable, synthetic polymer that is FDA-approved, thereby substantiating the clinical translatability of LC-NPs [29]. The hydrophilic surfaces of LC-NPs assist in evasion of the immune response and prolongation of systemic circulation [30]. Therefore, LC-NPs hold remarkable potential for translation to clinical studies of both oncologic and non-oncologic diseases of the kidney.

Following our preliminary *in vitro* studies that confirmed HK-2 proximal tubular cells internalized LC-NPs selectively *in vitro*, we found that LC-NPs could traffic selectively to the kidneys *in vivo* following injection into mice. Virtual absence of localization of LC-MPs to the kidneys supports a size-selective biodistribution, and the presence of LC-NPs in the glomerulus and tubular lumen immediately following injection indicates that LC-NPs are likely filtered through the glomerulus into the urinary space, where they descend into the tubular lumen, prior to their internalization by PTECs. The distribution of LC-NPs at the brush border of the proximal tubular epithelium and inside the apical membrane of the PTECs also indicates the likelihood that they are re-absorbed by the PTECs from the urinary space. As mentioned previously, megalin is expressed only at the apical membrane [2], and thus it represents the most probable receptor in the PTECs that binds to LC-NPs. Our important finding that LC-NPs remain in the kidneys for at least 7 days following a single injection reinforces a major advantage of nanomedicine, which is retention of the payload at the intended site of action, long after the administration of NPs. This property of LC-NPs could reduce effectively the dosing of the agents that are delivered by the NPs, an important feature that may limit the off-target toxicity of the encapsulated agent.

Reduced trafficking of LC-NPs to the kidneys of mice treated with cilastatin, a drug that binds to megalin and competitively inhibits the uptake of other drugs that bind to this protein [23], substantiates that megalin is the receptor to which LC-NPs bind in order to enter the PTECs. We cannot definitely rule out the theory that some LC-NPs may undergo transcytosis through peritubular capillary endothelial cells and internalization into PTECs through the basolateral membrane, a pathway that has been suggested by Daniel Heller's group for mesoscale nanoparticles [31, 32]. However, the restriction on trafficking to the kidneys imparted by treatment with cilastatin, along with our observation that LC-NPs are located along the apical membrane of PTECs immediately following injection, suggests that the majority of the LC-NPs are filtered through the glomerulus and re-absorbed from the urinary space. Similarly, in a recent report by Geng *et al.*, chitosan-modified nanoparticles with an average hydrodynamic diameter of 74 nm localized to the proximal tubule

epithelium of the kidneys in mice, a pathway the authors postulated was dependent on their filtration through the glomeruli [33]. Moreover, the inhibitory effect of cilastatin on the internalization of LC-NPs by PTECs was recapitulated by testing the uptake of LC-NPs by HK-2 cells *in vitro*. Furthermore, the identity of megalin as the ligand on the PTECs to which LC-NPs bind was substantiated by our findings that knockdown of its expression in HK-2 cells by siRNA interfered with their internalization of LC-NPs *in vitro*.

The functional versatility of LC-NPs is underlined by their selective trafficking to RCC. The higher accumulation of unconjugated NPs in the RCC tumor in comparison to the kidneys of unconjugated NP-treated mice in Fig. 2 likely reflects the dense vascularity and structure of the tumor. Thus, as the tumor is highly vascular and forms a condensed mass, higher accumulation of both unconjugated NPs and LC-NPs at day 1 was observed, a finding resembling the phenomenon known as the enhanced permeability and retention (EPR) effect that is ascribed commonly to tumors. However, at later time points, the tumors did not contain unconjugated NPs but retained LC-NPs (Fig. 5A–B), likely due to the specific binding of LC-NPs to megalin-expressing RCC and their subsequent internalization inside the cells. Injection of LC-NPs in mice bearing RCC identified the exophytic renal mass, which is the primary radiological finding in RCC patients. The recommendations for schedule of imaging following local resection of the primary tumor released by the National Comprehensive Cancer Network and American Urological Association result in identification of just 68.2% and 66.9% of recurrent lesions [34], respectively. In addition, the majority (~83%) of recurrent disease presents in patients within 5 years following resection [35]. Hence, a non-invasive method of identification for subclinical RCC lesions that evade detection by the typical imaging techniques currently in use at the time of diagnosis is sorely needed. Injection of LC-NPs containing the corresponding contrast media or dye prior to the imaging study (such as a gadolinium-based agent for magnetic resonance imaging) could improve this capability in the future, though additional studies are required to establish their selectivity of localization to the RCC tumor versus benign tumors. Therefore, LC-NPs could augment potentially the sensitivity of surveillance imaging performed for detection of recurrence, and for active monitoring of tumors in patients deemed to be at prohibitively high surgical risk [36] or for those at high risk of recurrence due to positive surgical margins [37]. Thus far, the only selective diagnostic imaging agent that has been described for RCC is a DOTA-conjugated molecule known as [^{111}In]XYIMSR-01 that binds to carbonic anhydrase IX and has been used to target human RCC xenografts in mice using single photon emission computed tomography (SPECT), where it is retained for up to 48 hours [38]. However, due to its rapid urinary excretion, this probe lacks the versatile potential of LC-NP for additional use as a platform for delivery for targeted therapeutic agents to the kidney.

Previous studies have demonstrated the overexpression of megalin in clear cell and papillary RCC [39–42]. Herein, we confirmed that human RCC expresses megalin not only in the primary tumor, but in metastatic lesions that have invaded the lymph node as well. DLNs of the kidney are common sites for metastasis, and the presence of DLN-positive disease is associated independently with poorer outcomes, including a decrease in the 5-year survival rate of patients from 75–95% to 5–35% [43]. DLN involvement also automatically increases

the cancer staging to Stage III, regardless of the size of the primary tumor, again reflecting the importance of metastasis to DLNs on clinical outcomes.

The presence of megalin in human RCC metastases and the trafficking of LC-NPs to the DLNs of kidneys implanted with RCC tumors reinforces the remarkable potential for LC-NPs to increase the sensitivity for detection of these metastatic lesions that commonly present subclinically and could serve thereby as a guide for more definitive local resection.

A major unmet need for the development of PTEC-targeted nanomedicine pervades the practice of clinical nephrology, as acute kidney injury affects up to 20% of all hospitalized patients worldwide [44] and results commonly from dysfunction of the proximal tubule due to ischemiareperfusion injury, sepsis, or drug-related toxicity [45]. Usage of LC-NPs could assist in solving this problem by concentrating the delivery of drugs developed in the future to treat these disorders at their intended site of action. Moreover, the field of nanomedicine contains a dearth of *in vivo* studies that have demonstrated the successful active targeting to PTECs of NPs conjugated with a molecular recognition entity [6, 7]. Hence, LC-NPs demonstrate remarkable potential as kidney-targeted drug carriers that not only deliver a concentrated therapeutic payload to PTECs, but also optimize pharmacokinetics due to their persistence in the kidney.

The development of targeted drug carriers to PTECs can also alter fundamentally the management of patients with PKD, a genetic condition that arises partially from the proximal tubule, affects between 1:400 and 1:1000 patients, and accounts for 5% of all patients who develop end-stage kidney disease requiring renal replacement therapy in the United States [46, 47]. The enthusiasm for recent evidence demonstrating the efficacy of the vasopressin-receptor 2 (V2R) antagonist tolvaptan in treating PKD patients at high risk of kidney disease progression has been tempered by its risk of liver toxicity, hypernatremia, and major drug interactions [48]. Hence, several clinical trials are underway to test other drugs, including the tyrosine kinase inhibitor tesevatinib (NCT03203642) [48], an anti-proliferative agent intended to limit cyst growth by targeting tubular epithelial cells, such as PTECs. Also, as overproduction of microRNAs--products of introns in the genome that silence functional mRNAs-has been implicated in the pathogenesis of PKD, the development of synthetic oligonucleotides called antimirs that bind and inhibit these microRNAs may hold relevance as targeted therapies for PKD in the future [49]. Another rarer disorder that affects the proximal tubule is type 2 renal tubular acidosis (RTA), which can occur in certain cases from inherited mutations in the gene *SLC4A4* that governs the synthesis of the basolateral sodium bicarbonate transporter NBCe1 [50]. LC-NPs could be used to encapsulate antimirs to augment their efficacy for PKD as well as to deliver gene therapy for PKD and type 2 RTA in the coming years.

Chronic exposure to toxic light chains is known to cause kidney disease through formation of casts in the tubular lumens and direct effect on the tubular epithelial cells in diseases such as multiple myeloma [20–22], a potential limitation to the clinical application of LC-NP. However, we demonstrated no significant immediate toxicity to the human proximal tubular cell line HK-2 *in vitro* following incubation with LC-NPs and no significant chronic damage to the kidneys of LC-NP-treated mice following one month of repetitive dosing *in vivo*,

perhaps because the total amount of light chains delivered to the PTECs did not exceed the critical threshold required to cause toxicity, or modification of the light chains prior to conjugation may have reduced their pathogenicity.

A potential limitation of the use of LC-NP could be its simultaneous targeting of benign proximal tubule epithelium, along with its localization to remote lesions of RCC. Therefore, the size of LC-NP can be increased in future studies to limit its targeting of the kidney, while preserving its capacity to localize to RCC. At this juncture, we foresee the immediate clinical utility of LC-NP for RCC as mainly that of a diagnostic agent that could be used to detect remote, subclinical, and recurrent lesions. This important function would address an urgent and unfulfilled clinical need.

In summary, we have synthesized LC-NPs, nanocarriers with the capability for the first time to target selectively both the PTECs of the kidney and RCC through the binding of light chains to megalin. Currently unmet, exigent clinical needs exist for improvement in the sensitivity of imaging techniques for the detection of RCC as well as for the treatment of kidney diseases that arise from the proximal tubule. Thus, LC-NPs demonstrate great potential for future use in the diagnosis of both non-oncologic and oncologic disorders that arise from the kidney.

Supplementary Material

Refer to Web version on PubMed Central for supplementary material.

Acknowledgments

The authors would like to thank Yarong Sunny Lu (InVivoEx, Boston, MA) for cutting and staining tissue sections with H&E. They would also like to thank Dr. Barry Brenner and Dr. Helmut Rennke for their guidance. The work in this study was supported by a research grant from Dialysis Clinic, Inc. (V.K.), and National Institutes of Health grants T32DK007527 (V.K.) and K08DK124685 (V.K.). F.O., V.K., and R.A. designed the study; F.O., V.K., M.U., A.A., S.J., O.A.Y., L.D., J. Z., B.B., and T.I. carried out the experiments; F.O., V.K., and R.A. analyzed the data; F.O. and V.K. made the figures; F.O., V.K., P.F., N.A., and R.A. drafted and revised the paper; all authors approved the final version of the manuscript. All authors declare that they have no competing interests. All data needed to evaluate the conclusions in the paper are present in the paper and/or the Supplementary Materials. Additional data are available from the authors upon request.

References

[1]. Farokhzad OC, Langer R, ACS Nano, 3 (2009) 16–20. [PubMed: 19206243]

[2]. Eshbach ML, Weisz OA, Annual review of physiology, 79 (2017) 425–448.

[3]. Patard JJ, Leray E, Rioux-Leclercq N, Cindolo L, Ficarra V, Zisman A, De La Taille A, Tostain J, Artibani W, Abbou CC, Lobel B, Guille F, Chopin DK, Mulders PF, Wood CG, Swanson DA, Figlin RA, Belldegrun AS, Pantuck AJ, Journal of clinical oncology : official journal of the American Society of Clinical Oncology, 23 (2005) 2763–2771. [PubMed: 15837991]

[4]. Speed JM, Trinh QD, Choueiri TK, Sun M, Curr Urol Rep, 18 (2017) 15. [PubMed: 28213859]

[5]. Janzen NK, Kim HL, Figlin RA, Belldegrun AS, The Urologic clinics of North America, 30 (2003) 843–852. [PubMed: 14680319]

[6]. Williams RM, Jaimes EA, Heller DA, Kidney international, 90 (2016) 740–745. [PubMed: 27292222]

[7]. Kamaly N, He JC, Ausiello DA, Farokhzad OC, Nature reviews. Nephrology, 12 (2016) 738–753. [PubMed: 27795549]

[8]. Wang J, Poon C, Chin D, Milkowski S, Lu V, Hallows K, Chung EJ, Nano Research, 11 (2018) 5584–5595.

[9]. Leheste JR, Rolinski B, Vorum H, Hilpert J, Nykjaer A, Jacobsen C, Aucouturier P, Moskaug JO, Otto A, Christensen EI, Willnow TE, The American journal of pathology, 155 (1999) 1361–1370. [PubMed: 10514418]

[10]. Verroust PJ, Christensen EI, Nephrology Dialysis Transplantation, 17 (2002) 1867–1871.

[11]. Marzolo M-P, Farfán P, Biological Research, 44 (2011) 89–105. [PubMed: 21720686]

[12]. Christensen EI, Birn H, Nature Reviews Molecular Cell Biology, 3 (2002) 258–267.

[13]. Klassen RBS, Allen PL, Batuman V, Crenshaw K, Hammond TG, Journal of Applied Physiology, 98 (2005) 257–263. [PubMed: 15286052]

[14]. Zhu F, Sun B, Wen Y, Wang Z, Reijo Pera R, Chen B, Stem Cells Dev, 23 (2014) 2119–2125. [PubMed: 24800694]

[15]. Kasinath V, Yilmam OA, Uehara M, Jiang L, Ordikhani F, Li X, Salant DJ, Abdi R, Kidney International, 95 (2019) 310–320. [PubMed: 30522766]

[16]. Liu P, O'Mara BW, Warrack BM, Wu W, Huang Y, Zhang Y, Zhao R, Lin M, Ackerman MS, Hocknell PK, Chen G, Tao L, Rieble S, Wang J, Wang-Iverson DB, Tymiak AA, Grace MJ, Russell RJ, Journal of the American Society for Mass Spectrometry, 21 (2010) 837–844. [PubMed: 20189823]

[17]. Conner KP, Rock BM, Kwon GK, Balthasar JP, Abuqayyas L, Wienkers LC, Rock DA, Drug Metabolism and Disposition, 42 (2014) 1906–1913. [PubMed: 25209366]

[18]. Meng F, Wang J, Ping Q, Yeo Y, ACS Nano, 12 (2018) 6458–6468. [PubMed: 29920064]

[19]. Gustafson HH, Holt-Casper D, Grainger DW, Ghandehari H, Nano today, 10 (2015) 487–510. [PubMed: 26640510]

[20]. Myatt EA, Westholm FA, Weiss DT, Solomon A, Schiffer M, Stevens FJ, Proc Natl Acad Sci U S A, 91 (1994) 3034–3038. [PubMed: 8159701]

[21]. Sanders PW, J Lab Clin Med, 124 (1994) 484–488. [PubMed: 7930873]

[22]. Ying WZ, Li X, Rangarajan S, Feng W, Curtis LM, Sanders PW, J Clin Invest, 130 (2019) 2792–2806.

[23]. Hori Y, Aoki N, Kuwahara S, Hosojima M, Kaseda R, Goto S, Iida T, De S, Kabasawa H, Kaneko R, Aoki H, Tanabe Y, Kagamu H, Narita I, Kikuchi T, Saito A, Journal of the American Society of Nephrology : JASN, 28 (2017) 1783–1791. [PubMed: 28052987]

[24]. Conti S, Perico L, Grahammer F, Huber TB, Current opinion in nephrology and hypertension, 26 (2017) 148–153. [PubMed: 28212178]

[25]. Gagliardini E, Conti S, Benigni A, Remuzzi G, Remuzzi A, Journal of the American Society of Nephrology : JASN, 21 (2010) 2081–2089. [PubMed: 21030599]

[26]. Wartiovaara J, Ofverstedt LG, Khoshnoodi J, Zhang J, Makela E, Sandin S, Ruotsalainen V, Cheng RH, Jalanko H, Skoglund U, Tryggvason K, The Journal of clinical investigation, 114 (2004) 1475–1483. [PubMed: 15545998]

[27]. Grahammer F, Nesterov V, Ahmed A, Steinhardt F, Sandner L, Arnold F, Cordts T, Negrea S, Bertog M, Ruegg MA, Hall MN, Walz G, Korbmacher C, Artunc F, Huber TB, The Journal of clinical investigation, 126 (2016) 1773–1782. [PubMed: 27043284]

[28]. Chang RL, Ueki IF, Troy JL, Deen WM, Robertson CR, Brenner BM, Biophysical journal, 15 (1975) 887–906. [PubMed: 1182263]

[29]. Gentile P, Chiono V, Carmagnola I, Hatton PV, Int J Mol Sci, 15 (2014) 3640–3659. [PubMed: 24590126]

[30]. Xu X, Ho W, Zhang X, Bertrand N, Farokhzad O, Trends in molecular medicine, 21 (2015) 223–232. [PubMed: 25656384]

[31]. Williams RM, Shah J, Ng BD, Minton DR, Gudas LJ, Park CY, Heller DA, Nano Lett, 15 (2015) 2358–2364. [PubMed: 25811353]

[32]. Williams RM, Shah J, Tian HS, Chen X, Geissmann F, Jaimes EA, Heller DA, Hypertension, 71 (2018) 87–94. [PubMed: 29133360]

[33]. Geng X, Zhang M, Lai X, Tan L, Liu J, Yu M, Deng X, Hu J, Li A, Advanced healthcare materials, 7 (2018) e1800558. [PubMed: 30277665]

[34]. Stewart SB, Thompson RH, Psutka SP, Cheville JC, Lohse CM, Boorjian SA, Leibovich BC, J Clin Oncol, 32 (2014) 4059–4065. [PubMed: 25403213]

[35]. Adamy A, Chong KT, Chade D, Costaras J, Russo G, Kaag MG, Bernstein M, Motzer RJ, Russo P, J Urol, 185 (2011) 433–438. [PubMed: 21167521]

[36]. Smaldone MC, Kutikov A, Egleston BL, Canter DJ, Viterbo R, Chen DY, Jewett MA, Greenberg RE, Uzzo RG, Cancer, 118 (2012) 997–1006. [PubMed: 21766302]

[37]. Shah PH, Moreira DM, Okhunov Z, Patel VR, Chopra S, Razmaria AA, Alom M, George AK, Yaskiv O, Schwartz MJ, Desai M, Vira MA, Richstone L, Landman J, Shalhav AL, Gill I, Kavoussi LR, J Urol, 196 (2016) 327–334. [PubMed: 26907508]

[38]. Yang X, Minn I, Rowe SP, Banerjee SR, Gorin MA, Brummet M, Lee HS, Koo SM, Sysa-Shah P, Mease RC, Nimmagadda S, Allaf ME, Pomper MG, Oncotarget, 6 (2015) 33733–33742. [PubMed: 26418876]

[39]. Schuetz AN, Yin-Goen Q, Amin MB, Moreno CS, Cohen C, Hornsby CD, Yang WL, Petros JA, Issa MM, Pattaras JG, Ogan K, Marshall FF, Young AN, The Journal of molecular diagnostics : JMD, 7 (2005) 206–218. [PubMed: 15858144]

[40]. Dupasquier S, Delmarcelle A-S, Marbaix E, Cosyns J-P, Courtoy PJ, Pierreux CE, BMC Molecular Biology, 15 (2014) 9. [PubMed: 24885929]

[41]. Young AN, Master VA, Amin MB, TheScientificWorldJournal, 6 (2006) 2505–2518.

[42]. Gonias SL, Karimi-Mostowfi N, Murray SS, Mantuano E, Gilder AS, PloS one, 12 (2017) e0186649–e0186649. [PubMed: 29088295]

[43]. Jamal JE, Jarrett TW, International journal of surgical oncology, 2011 (2011) 816926. [PubMed: 22312526]

[44]. Susantitaphong P, Cruz DN, Cerda J, Abulfaraj M, Alqahtani F, Koulouridis I, Jaber BL, Acute N Kidney Injury Advisory Group of the American Society of, Clin J Am Soc Nephrol, 8 (2013) 1482–1493. [PubMed: 23744003]

[45]. Laurent G, Kishore BK, Tulkens PM, Biochem Pharmacol, 40 (1990) 2383–2392. [PubMed: 2268362]

[46]. Torres VE, Harris PC, Kidney international, 76 (2009) 149–168. [PubMed: 19455193]

[47]. Harris PC, Torres VE, Annual review of medicine, 60 (2009) 321–337.

[48]. Cornec-Le Gall E, Alam A, Perrone RD, Lancet, 393 (2019) 919–935. [PubMed: 30819518]

[49]. Hajarnis S, Lakhia R, Patel V, MicroRNAs and Polycystic Kidney Disease, in: Li X (Ed.) Polycystic Kidney Disease, Brisbane (AU), 2015.

[50]. IGARASHI T, INATOMI J, SEKINE T, SEKI G, SHIMADZU M, TOZAWA F, TAKESHIMA Y, TAKUMI T, TAKAHASHI T, YOSHIKAWA N, NAKAMURA H, ENDOU H, Journal of the American Society of Nephrology, 12 (2001) 713–718. [PubMed: 11274232]

Highlights

- Light chain-conjugated nanoparticles (LC-NPs) interact selectively with proximal tubule epithelial cells (PTECs) in the kidney.
- Systemic administration of LC-NPs to mice resulted in their specific retention by megalin-expressing PTECs for seven days.
- The primary tumor and lymph nodes metastases of human renal cell carcinoma express megalin, reinforcing the potential of LC-NPs for clinical use.

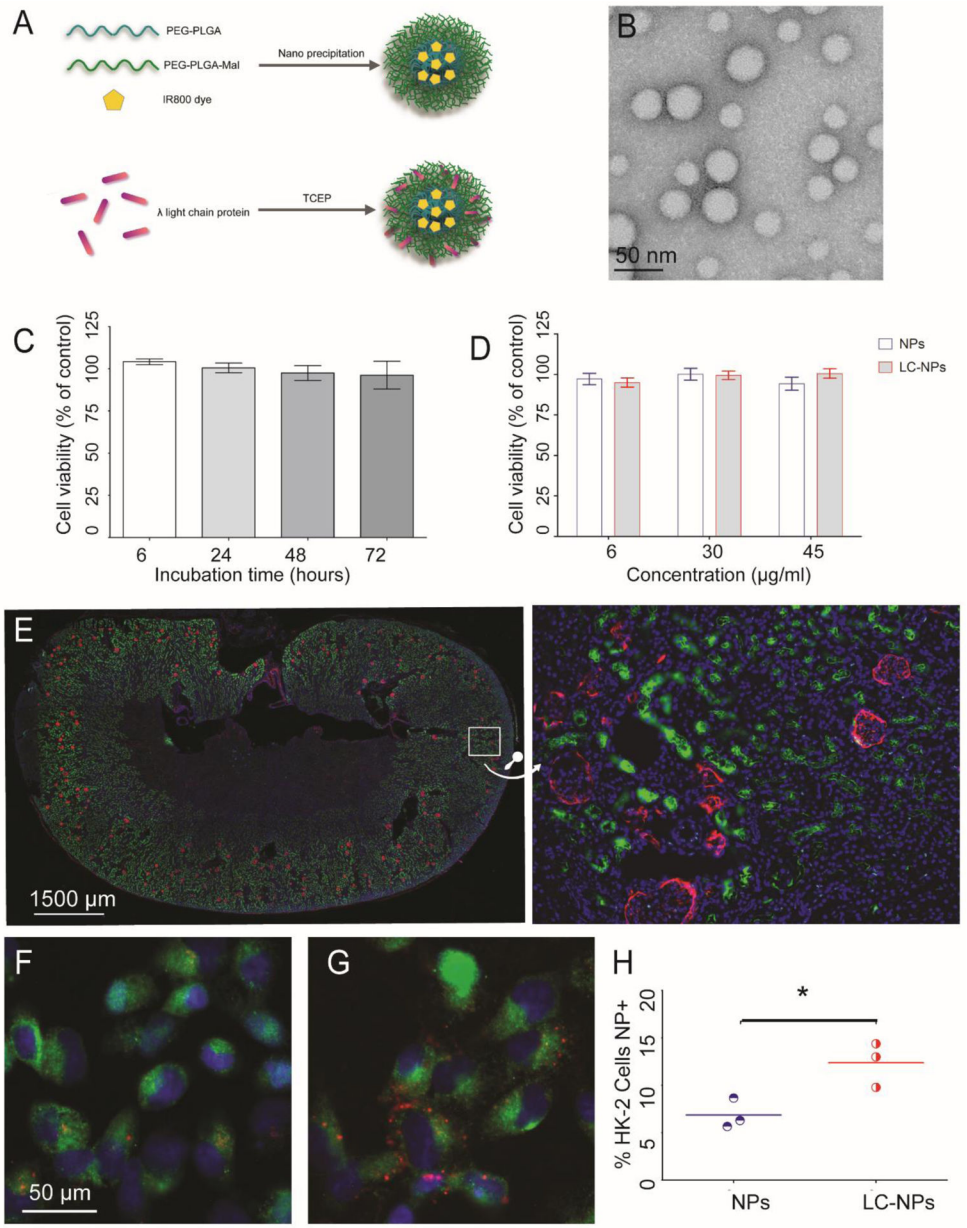

Figure 1. Characterization and internalization of LC-NPs by megalin-expressing PTECs *in vitro*.

(A) Schematic of fabrication and conjugation of LC-NP. (**B**) Representative transmission electron micrograph (TEM) of LC-NPs, negatively stained and imaged at 80.0 kV (scale bar: 50 nm), reveals their uniform spherical shape. **(C)** Exposure of HK-2 cells to LC-NPs for 6, 24, 48, and 72 hours demonstrated no significant difference in viability between the time points, as measured by MTT assay (n=8 replicates/condition). **(D)** Incubation of HK-2 cells with different concentration of either NPs or LC-NPs for 24 hours demonstrated no significant difference in viability, as assessed by MTT assay (n=8 replicates/condition). The data are representative of 2 independent MTT assays. **(E)** Representative fluorescence micrographs at low and high magnification of a murine kidney demonstrated expression of megalin (green) by the proximal tubules, situated along their apical surface. Sections were

also stained with glomerular marker podoplanin (red) and nuclear marker 4',6-diamidino-2-phenylindole (DAPI, blue). Fluorescence micrographs of HK-2 cells incubated with **(F)** NPs (red) and **(G)** LC-NPs (red) for one hour showed a significantly higher accumulation of LC-NPs in comparison to NPs. Cells were stained for megalin (green) and with nuclear marker DAPI (blue). (**H**) A higher percentage of LC-NPs was uptaken by HK-2 cells compared to NPs (n=3). Values are means ± SD. **P<0.05* as calculated by two-tailed Student's t-test.

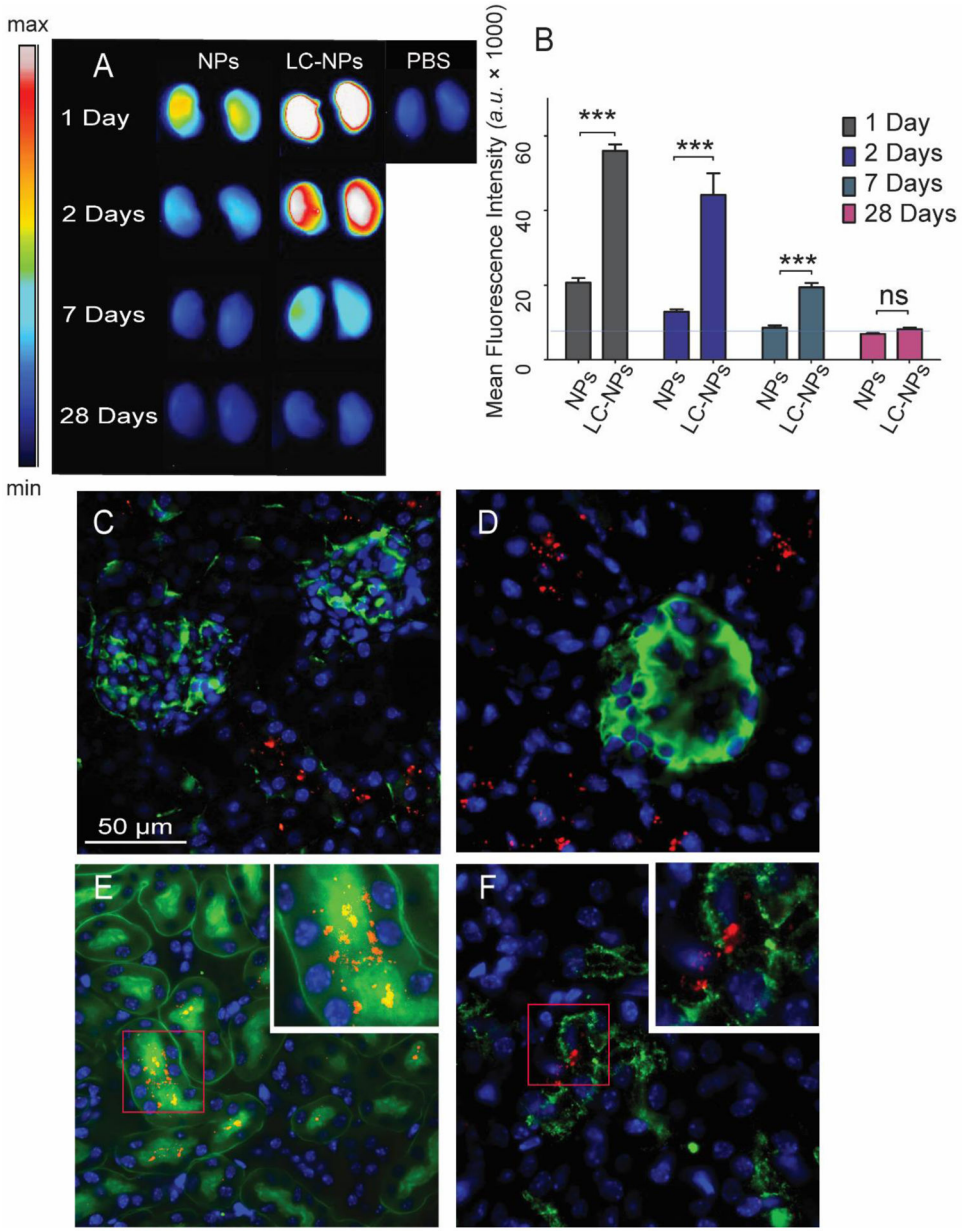

Figure 2. ***Ex vivo*** **trafficking and biodistribution of LC-NPs in murine kidney.**

(A) Representative *ex vivo* images of murine kidneys 1, 2, 7, and 28 days following intravenous injection of unconjugated NPs or LC-NPs, or 1 day following intravenous injection of PBS. **(B)** A significantly higher signal was observed in kidneys from mice injected with LC-NPs in comparison to NPs, as indicated by MFI (n=3–4/group). Fluorescence micrographs of kidneys harvested from mice 24 hours following injection of LC-NPs (red) demonstrating their localization to the proximal tubule, as indicated by staining with **(C)** vascular marker CD31 (green), **(D)** glomerular marker podoplanin (green), and proximal tubular markers **(E)** LTL (green) as well as **(F)** megalin (green). Insets in **(E)** and **(F)** indicate localization of LC-NPs to the apical half of the PTECs. Values are means ± SD. ****P<0.005* and ns: not significant as calculated by two-tailed Student's t-test.

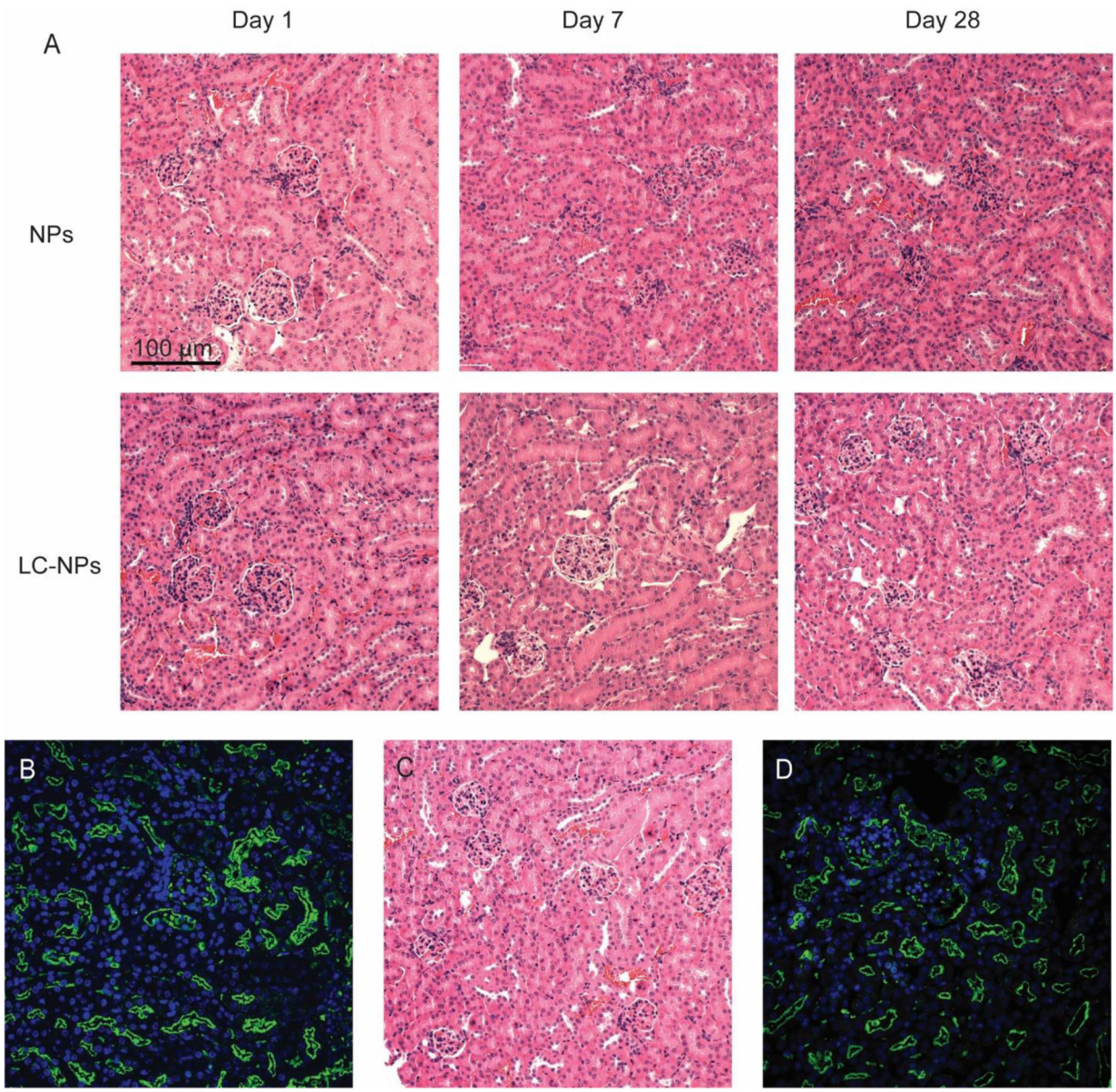

Figure 3. Assessment of toxicity of LC-NPs.

(A) Light micrograph of H&E-stained kidney tissues harvested from LC-NPs and NPs-treated mice at 1, 7, and 28 days following injection, showing normal glomerular and tubular architecture (n=4 mice). **(B)** A representative image of immunofluorescence staining for KIM-1 staining in kidney at day 7 post injection, demonstrating no sign of damage in proximal tubular architecture of the kidney tissues (n=4 mice). **(C)** A representative light micrograph of H&E-stained kidney tissue from repetitive injection of LC-NPs, showing no change in morphology (n=5 mice). **(D)** A representative image of immunofluorescence staining for KIM-1 staining in kidney tissue from repetitive injection of LC-NPs, showing no sign of damage in proximal tubular architecture of the kidney tissues (n=5 mice). Megalin in green, KIM-1 in red, and DAPI in blue.

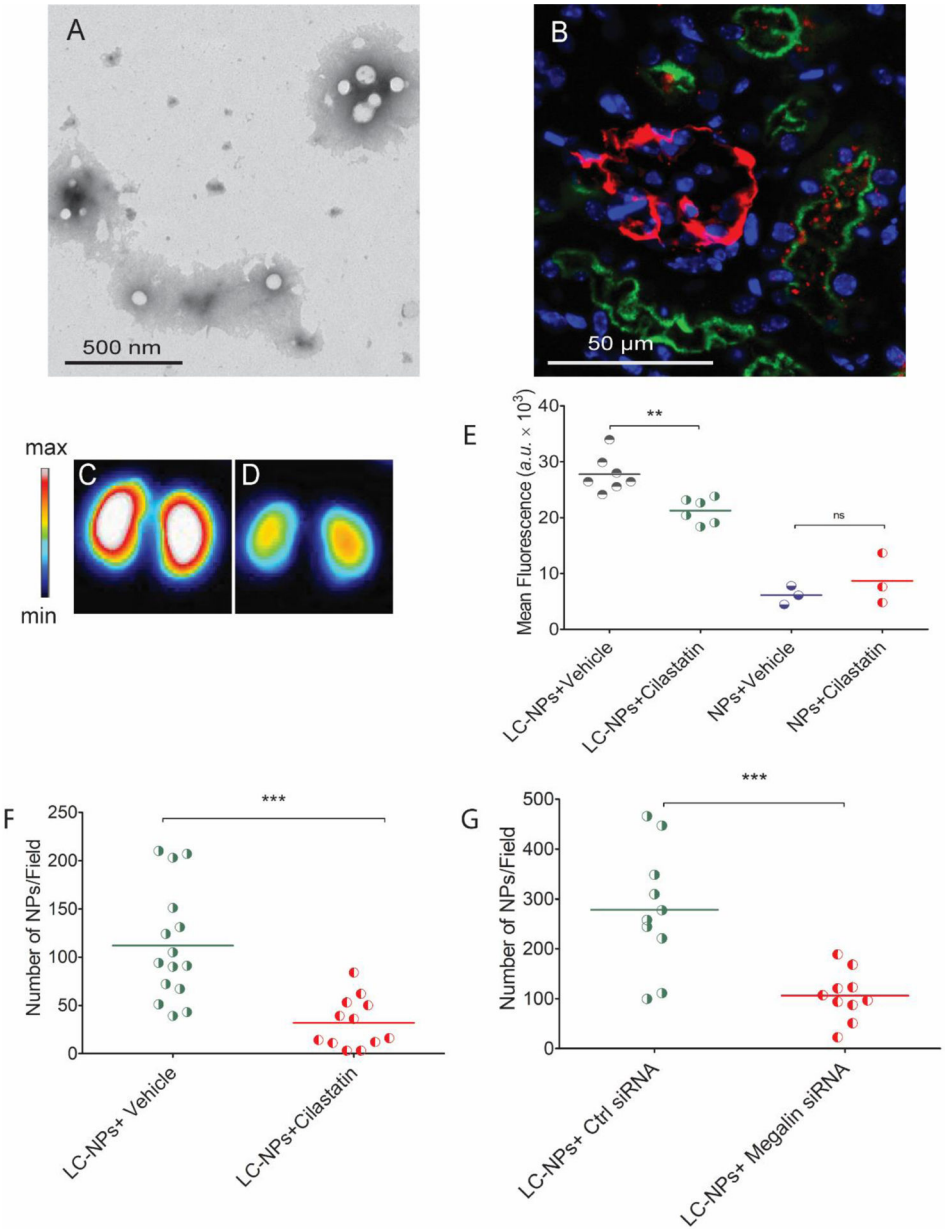

Figure 4. Interrogation of mechanism by which LC-NPs localize to PTECs.

(A) TEM micrograph of urine immediately after intravenous injection of LC-NPs demonstrating the presence of LC-NPs. (**B**) Representative fluorescence micrograph of kidney immediately after injection with LC-NPs (red) demonstrating distribution in proximal tubules, as indicated by co-staining with proximal tubule marker megalin (green) and nuclear marker DAPI (blue). (**C-D**) Representative *ex vivo* images of kidneys from mice treated with **(C)** vehicle (DPBS), and **(D)** cilastatin. **(E)** MFI of the kidneys from mice treated with either cilastatin or vehicle demonstrating significantly higher MFI in the kidneys from those treated with DPBS (n=3–7/group). **(F)** LC-NPs underwent lower uptake by HK-2 cells treated with cilastatin than vehicle (DPBS)-treated cells. **(G)** HK-2 cells treated with megalin siRNA also exhibited lower uptake of LC-NPs in comparison to those

treated with control siRNA. Values are means ± SD. means ± SD. ***P<0.01,* and ****P<0.001* and ns: not significant as calculated by two-tailed Student's t-test.

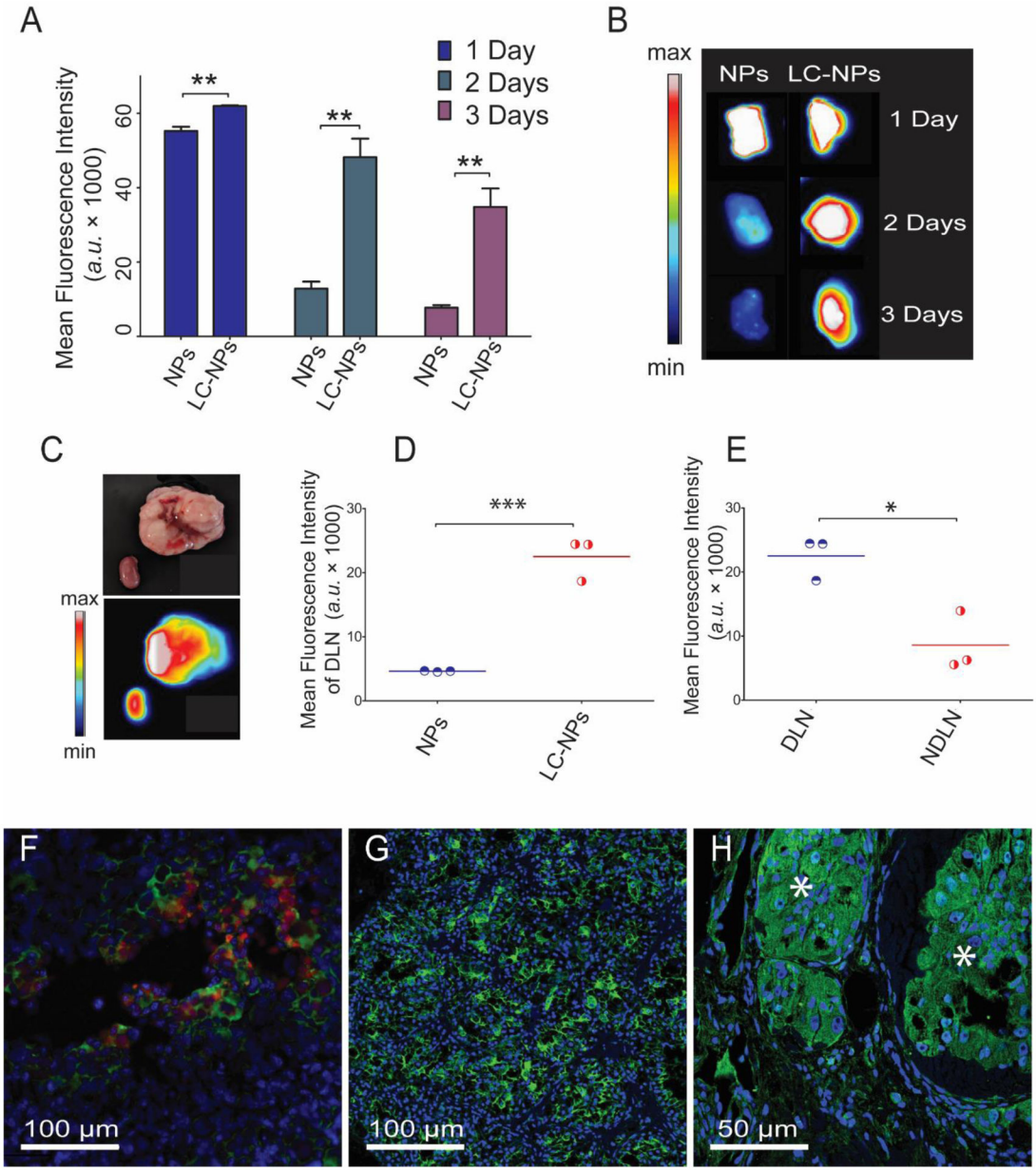

Figure 5. Trafficking of LC-NPs to megalin-expressing RCC in mice.

(A) MFI of kidneys containing RCC at 1, 2, 3 days following intravenous injection of either NPs or LC-NPs in tumor-bearing mice demonstrates significantly higher signal in LC-NP-injected mice compared to NP-injected mice. **(B)** Representative images of kidneys with tumors from euthanized mice at the designated time points. **(C)** Representative photograph and *ex vivo* image demonstrating MFI of kidney with RCC (on right) and contralateral kidney without RCC (on left) 24 hours following injection of LC-NPs. (**D**) MFI of the kidney-draining lymph nodes (DLNs) of the RCC tumor-bearing mice confirms higher retention of LC-NPs compared to unconjugated NPs at 3 days post-injection. (**E**) DLNs exhibit higher signal compared to NDLNs at 3 days following injection of LC-NPs. (n=3–4/group) **(F)** A representative fluorescence micrograph of murine tumor tissue exhibits co-

localization of LC-NPs (red) with megalin (green)-expressing cells in tumor tissue. Nuclear marker DAPI (blue). **(G)** A representative fluorescence micrograph of human RCC depicts high expression of megalin (green) in the tumor. Nuclear marker DAPI (blue). **(H)** A representative fluorescence micrograph of human DLN depicts high expression of megalin (green) in clearly demarcated metastatic lesions of RCC (asterisks). Values are means ± SD. *$P<0.05$, **$P<0.01$, and ***$P<0.001$, as calculated by two-tailed Student's t-test.

Table 1.

Renal function of C57BL/6 mice injected with either NPs or LC-NPs (n=4).

	BUN at Day 1 (mg/dL)	BUN at Day 7 (mg/dL)	BUN at Day 28 (mg/dL)
NP	15.5±1	14.5±1.3	15.2±4.15
LC-NP	15.6±3.1	15.3±1.7	13.9±2.9

Table 2.

Renal function of C57BL/6 mice injected with either NPs or LC-NPs (n=4).

	Cr at Day 1 (mg/dL)	Cr at Day 7 (mg/dL)	Cr at Day 28 (mg/dL)
NP	0.15±0.02	0.11±0.06	0.14±0.02
LC-NP	0.15±0.06	0.08±0.04	0.14±0.01